Proceedings of Global Power and Propulsion Society
ISSN-Nr: 2504-4400
GPPS Xi'an21
18th–20th October, 2021

www.gpps.global

GPPS-TC-2021-0338

INFLUENCE OF AXIAL GAPS ON FORCED RESPONSE OF DIFFERENT MODE SHAPES IN A LOW-PRESSURE COMPRESSOR

Hye Rim Kim*†, Dajan Mimic†‡, and Joerg R. Seume†‡
†Institute of Turbomachinery and Fluid Dynamics
Leibniz Universität Hannover
*kim@tfd.uni-hannover.de
Garbsen, Germany
‡Cluster of Excellence SE²A – Sustainable and Energy Efficient Aviation
Technische Universität Braunschweig
Braunschweig, Germany

ABSTRACT

Forced-response vibrations present an ongoing challenge in compressor design. This is especially apparent when axial-gap variations are considered: narrower gaps come with the benefit of a lower component weight. From the standpoint of aeroelasticity, however, this typically causes a stronger wake-induced excitation. Conversely, recent results have demonstrated an increased excitation of certain mode shapes with increasing axial gap.

This paper investigates how the forced response of different mode shapes is affected by operating-point-related and design-related changes of the excitation source. Extensive time-linearised simulations are conducted at various off-design operating points with different mode shapes. Fourier-transformed gust boundary conditions are considered as the excitation source.

The reduced frequency is identified as the determining factor for the sensitivity of the aerodynamic work with respect to axial-gap variations. Three reduced-frequency regimes are identified: moderate sensitivity for low reduced frequencies, low sensitivity for moderate reduced frequencies, and high sensitivity for high reduced frequencies. The cases with an inverse behaviour of the aerodynamic work with respect to the axial-gap variation are shown to occur in the low-sensitivity regime. It is demonstrated that they are a result of changes in the interaction of the incoming wakes with the rotor potential field.

INTRODUCTION

Forced response is an aeroelastic phenomenon induced by a cyclic disturbance. Resonance occurs when the frequency of this unsteady disturbance matches the eigenfrequency of the blade. This can result in blade failure and is to be avoided. Forced-response excitation is, however, unavoidable in multi-stage turbomachinery environments, since blades always receive an unsteady aerodynamic load from neighbouring blade rows in the form of wakes, shocks, or potential fields. The most straightforward way of forced response-free operation would be to avoid specific rotational speeds where the periodic excitation matches the eigenfrequencies of the excited blades. However, this is almost impossible to achieve (Kielb and Chiang, 1992). This difficulty becomes especially challenging with the increasing demand for flexible engine operation. In many cases, gas turbines are required to operate near resonance points or to cross them during transients.

Manwaring and Wisler (1993) conducted substantial experimental and numerical studies in compressors and turbines to quantify the unsteady aerodynamic loading on blades. The authors showed that the assumption of a linear response yields reasonably accurate predictions of the unsteady loading in various configurations and operating points by comparing different numerical schemes. More recent investigations (Besem et al., 2016; Schoenenborn, 2018) applied non-linearised solvers in multi-stage and multi-passage environment. These solvers provided reasonably good agreement with time-domain unsteady Reynolds-averaged Navier–Stokes (RANS) for prediction of unsteady flow fields (Junge et al., 2015). The results showed that time-linearised methods might predict the unsteady-pressure blade loading inaccurately, if scattering modes occur between stages. These are, however, not considered in this paper in order to isolate the first-order stator-rotor interactions caused by impinging wakes.

The German Aerospace Center (Deutsches Zentrum für Luft- und Raumfahrt, DLR) presented a time-linearised RANS-equation solver (linearTRACE) as a numerical tool of aeroelasticity simulation about a decade ago (Kersken et al., 2012).

The applicability of linearTRACE in forced-response analyses was highlighted in a subsequent study, introducing a new gust boundary condition (Blocher and Gómez Fernández, 2014). Since then, this solver has been widely applied in aeroelasticity research. This numerical method has undergone continuous experimental validation at the Institute of Turbomachinery and Fluid Dynamics with respect to forced-response and aerodynamic-damping evaluation (Bittner et al., 2018; Meinzer and Seume, 2020).

Investigations regarding a variation of axial gap in turbomachinery blade rows have been widely conducted. A small axial gap is favourable because it reduces overall length of compressors and turbines. This can significantly alter aerodynamic performance, and more importantly, forced response of the components. The importance of axial gap study is not only derived from design perspective, but also provide satisfactory insight on how blade rows interact to each other. Korakianitis (1992*a*) and Korakianitis (1992*b*) investigated unsteady force on turbine blades in different axial gaps. The authors investigated the influence of wake and potential field models separately as well as in combination. Interestingly, it appears that the overall unsteady force does not always decrease as the gap increases. Chen et al. (2013) conducted a similar parametric study using 3D turbine blades, with similar results. However, the physical mechanism behind this has not yet been understood to the knowledge of the authors.

A previous study was initiated to investigate aerodynamic and aeroelastic performance in a low-pressure compressor of a ultra-high bypass-ratio (UHBR) engine (Eggers et al., 2020). Three different axial gaps were studied under the influence of realistic UHBR-specific inflow. The sensitivity of forced-response vibrations with respect to the unsteady-pressure sources from an upstream stator as well as the blade deformation were evaluated quantitatively by varying the axial gaps. Depending on the mode shape, the vibrational amplitude may increase or decrease with an increasing axial gap. This behaviour was explained by the position of maximum blade deflection. The necessity of a comprehensive study for a detailed analysis was addressed in that study.

The following objectives are derived from the previous works:

- Extension of the parametric study by Eggers et al. (2020) to include different operating points and mode shapes
- Quantitative comparison of the unsteady work on the blades with respect to an axial-gap variation
- Detailed analysis of the unsteady pressure and aerodynamic work
- Identification of deterministic parameters to predict forced-response behaviour

METHODOLOGY

In order to achieve objectives mentioned above, a comprehensive numerical study is conducted for the case of a low-pressure compressor. Three different axial gaps are considered at three different operating points (OP). The first six modes are applied to each axial gap and operating point. Detailed information regarding the compressor configuration and numerical setup are given below.

Compressor Configuration

The three-stage compressor in this study was designed at the Institute of Jet Propulsion and Turbomachinery (IFAS, Technische Universität Braunschweig) for the purpose of UHBR geared-turbofan engine research. A meridional view of the compressor, which has a distinctly low aspect ratio, is depicted in Fig. 1 together with an extended S-duct upstream. The S-duct provides UHBR-specific, significantly inhomogeneous compressor inlet flow, which is characterised by thick boundary layers and a strong radial distortion. Three configurations with different axial gaps are investigated. For the reference case, the axial gap between the stator and rotor row corresponds to 30% of the upstream stator chord. The gap varies by $\pm 10\%$ for the other configurations. Additional details can be found in (Eggers et al., 2020).

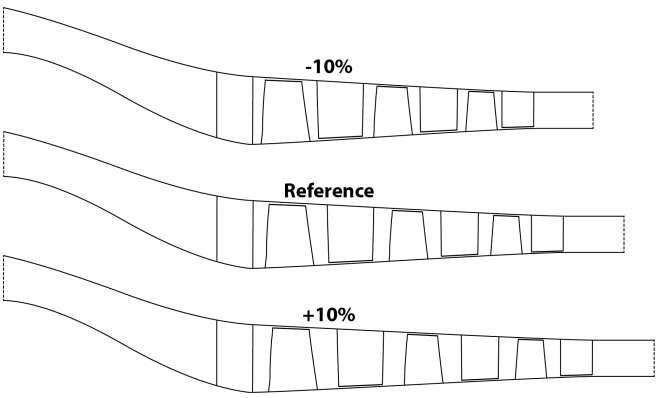

Figure 1 Different axial gaps in the meridional view (Eggers et al., 2020)

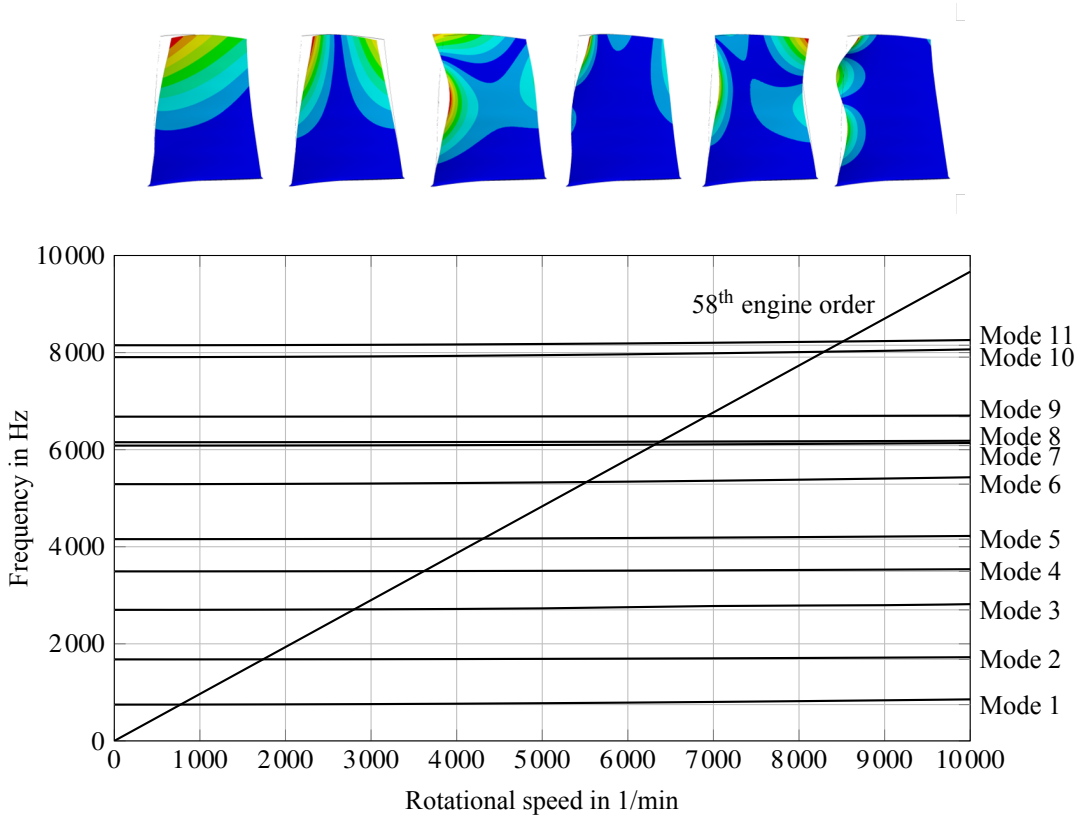

Figure 2 Mode shapes of the rotor blade for Mode 1 to Mode 6 (blue - no deformation, red - maximum deformation) and Campbell diagram

Numerical Setup

Time-linearised simulations require steady-state solutions as their initial state. For the aeroelasticity simulations, modal analyses are conducted using ANSYS Mechanical to acquire the resonance frequencies and mode shapes for the first six modes. Then, a new domain which contains only the target blade is extracted from a multi-stage simulation. The gust boundary condition is extracted from the outlet of the upstream stator in the steady-state RANS simulation and, after undergoing a spatial Fourier transform, subsequently imposed as an inlet boundary condition for the time-linearised simulation of the rotor. The blade deformation is mapped onto the blade surface to later calculate the unsteady work per area together with the unsteady pressure field. The unsteady pressure field, as well as other unsteady field variables, are computed from the time-linearised unsteady RANS equations, which are solved without considering the blade deformation. The solver linearTRACE, which was used in this work, includes only the first harmonic of any disturbance. The background of this approximation is explained in the first part of the results section.

The unsteady aerodynamic work per area follows from the dot product of the calculated unsteady blade-surface pressure and the blade deformation. Finally, the surface distribution of the unsteady work per area is integrated over the blade surface to obtain the aerodynamic work per cycle.

The forced-response amplitude is determined by the ratio of the aerodynamic forcing work to the energy dissipated by the aerodynamic damping. As documented by Eggers et al. (2020), the aerodynamic damping exhibits only 0..2% variation for the axial-gap changes considered. For this reason, the damping is omitted in this study and only the unsteady aerodynamic work per cycle is compared as a representative quantity of the forced-response behaviour. More details regarding the aeroelasticity tool chain used here can be found in Eggers et al. (2020).

Test Cases

The mode shapes investigated are shown in Fig. 2 together with the corresponding Campbell diagram. Mode 2 in OP1 (1738/min) and Mode 3 in OP2 (2804/min) were simulated and analysed by Eggers et al. (2020). These operating points were selected from a Campbell diagram where each eigenfrequency corresponds to the engine order determined by the upstream blade number. The study revealed that the aerodynamic work decreases with an increasing axial gap in the case of Mode 2 at OP1. However, Mode 3 showed the opposite trend at OP2.

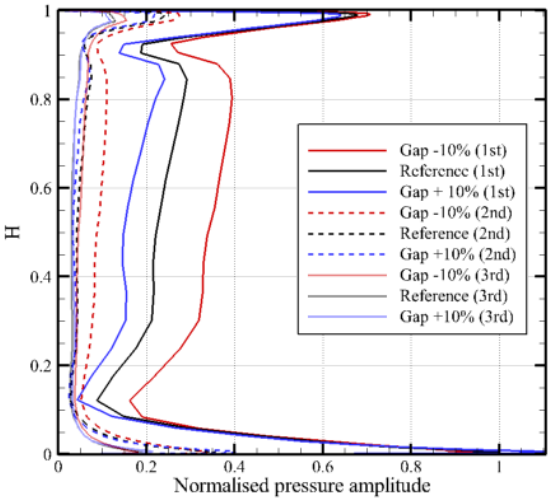

Figure 3 Amplitude of unsteady pressure in the gust boundary conditions at the rotor inlet

To eliminate the dependency on the operating points, Mode 3 was simulated at OP1 as well. In addition to that, different mode shapes from Mode 1 to Mode 6 were studied at OP1 as well as at another, higher rotor speed of 3618/min (OP3). In total, 39 cases, comprising 13 different reduced frequencies for three axial gaps of -10%, reference, and $+10\%$ were simulated. All cases considered are summarised in Tab. 1 together with their respective eigenfrequencies and reduced frequencies.

RESULTS AND DISCUSSION

Firstly, the gust boundary conditions are compared for different axial gaps to identify influencing harmonics and to quantify the unsteadiness of the excitation source. Secondly, the integrated aerodynamic work on the blades are presented and compared for different axial gaps. Lastly, the unsteady pressure and work distributions on the blade surfaces are analysed for selected cases together with the propagation of unsteady flow features throughout the rotor passages.

Comparison of Gust Boundary Conditions

Figure 3 shows the unsteady pressure amplitudes against the channel height. The values are extracted from the interface between the stator and rotor domain. The first three harmonics are depicted. The pressure is normalised with respect to the maximum pressure of the first harmonic from the reference case. Only the boundary conditions of OP1 are presented here, since the relative deviation from the reference is almost the same for the different axial gaps at OP2 and OP3. It can be seen that the unsteady pressure amplitude decreases with an increasing axial gap. Likewise, the lower unsteady pressure amplitudes in the freestream indicate weaker incoming wakes.

The inflow features thick boundary layers caused by the long upstream S-duct, as evidenced by the near-wall regions of high unsteadiness. The near-wall unsteadiness decreases in the tip region for larger axial gaps, whereas it decreases slightly in the hub region. The blade does, however, not deform at the hub, resulting in a vanishing aerodynamic work in this region.

As evidenced by the figure, the second and third harmonics are rather small in comparison with the first harmonic. The gap-dependent variations are even smaller for these higher harmonics. Hence, they do not contribute significantly to variations in the aerodynamic work and can be neglected in this work, which considers only the sensitivities with respect to gap variations. This also confirms the applicability of the linearised solver linearTRACE.

Table 1 Test cases with corresponding reduced frequencies

		Mode 1	Mode 2	Mode 3	Mode 4	Mode 5	Mode 6
	f	751 Hz	1680 Hz	2704 Hz	3493 Hz	4158 Hz	5293 Hz
1738/min (OP1)	k	1.19	2.67*	4.29	5.55	6.60	8.41
2804/min (OP2)	k			2.56*			
3618/min (OP3)	k	0.54	1.21	1.96	2.53*	3.01	3.83

*Crossing points from the Campbell diagram

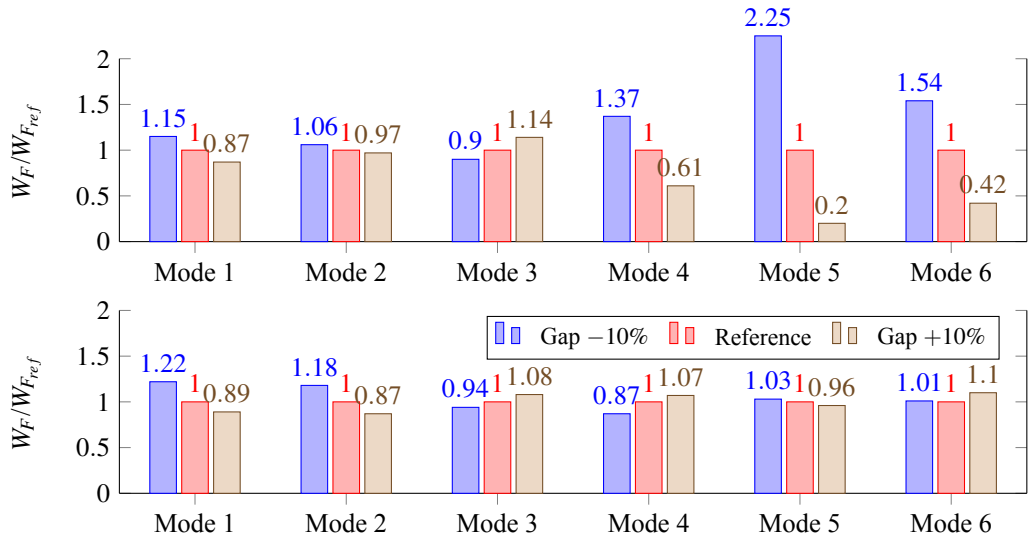

Figure 4 Relative aerodynamic work (top: OP1, bottom: OP3)

Overall Aerodynamic Work

The calculated aerodynamic work per cycle is summarised in Fig. 4. The aerodynamic work decreases with an increasing axial gap in the majority of cases. This trend is, however, reversed for Mode 3. Furthermore, Mode 4 and Mode 6 experience a trend reversal between OP1 and OP3. This behaviour implies that neither the operating point nor the mode shape can be determining parameters when a reduction of the vibrational response is to be achieved by controlling the axial gap.

Figure 5 shows the relative aerodynamic work W_F versus the reduced frequency k for all 39 cases. It is striking that the sensitivity of the aerodynamic work with respect to the axial-gap variation is not consistent throughout the investigated range of the reduced frequency: three distinct regimes appear. First, the sensitivity decreases up to $k = 1.96$. Then, for $k = 1.96..4.29$, the forced response varies by approximately $\pm 10\%$ with the axial gap variation of $\pm 10\%$. Within this low-sensitivity regime, four cases mentioned before exhibit an unintuitive, reversed trend, i.e., the aerodynamic work increases with the axial gap. Within $k = 4.29..6.64$, the sensitivity increases again, with a notable, steep rise starting from $k = 5.55$. Here, the case of $k = 6.64$ exhibits the highest sensitivity. The aerodynamic work is more than twice as large as that of the reference case.

The sensitivity regimes identified here, may be applicable to the compressor-design stage. Further investigations are, however, needed to obtain the generalisability necessary.

The sensitivity of the overall aerodynamic work on the blades was discussed in this section. In the following section, the radial distributions of the unsteady pressure and aerodynamic work are presented for selected cases.

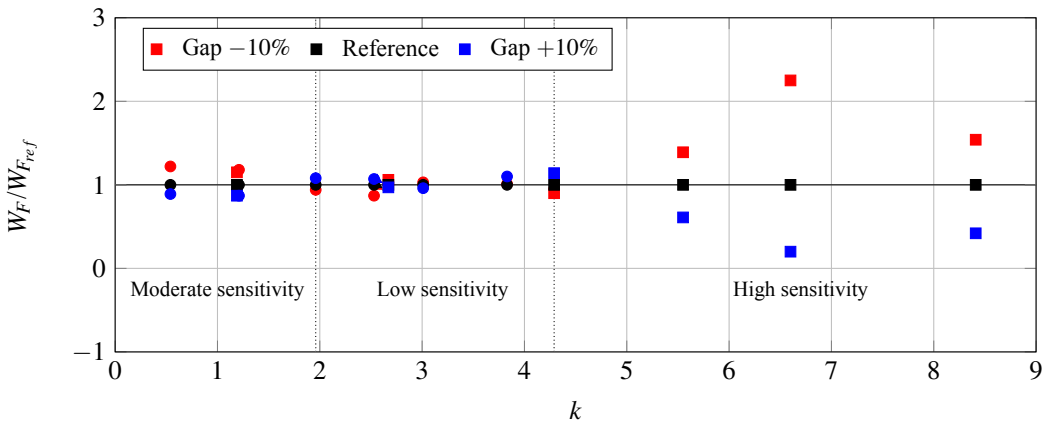

Figure 5 Relative aerodynamic work versus reduced frequency

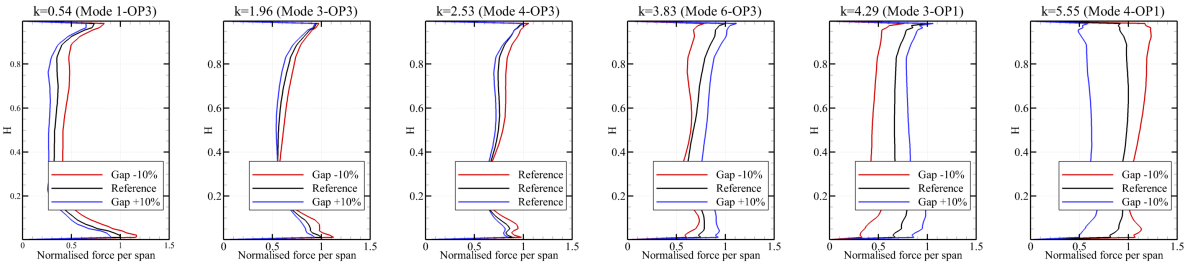

Figure 6 Radial distribution of chordwise-integrated pressure amplitude

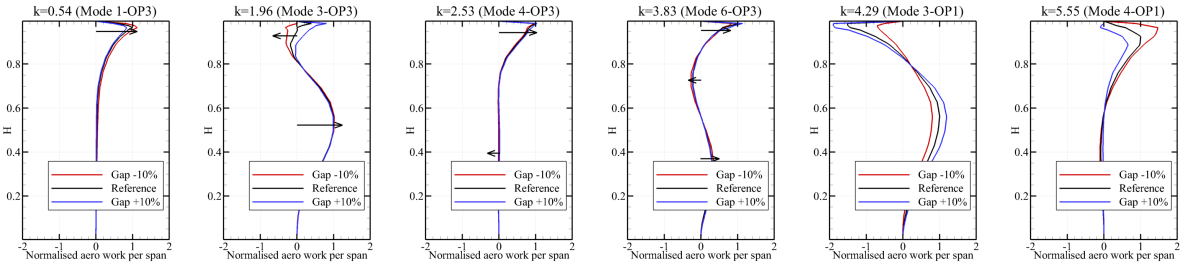

Figure 7 Radial distribution of chordwise-integrated aerodynamic work

Unsteady Pressure and Aerodynamic Work Distribution

Figures 6 and 7 show the spanwise distributions of the unsteady force per span, obtained from a chordwise integration of the pressure amplitude $\hat{p}$, together with the corresponding aerodynamic work per unit span w_F for selected cases. The parameters are integrated along the blade chord at each spanwise position, and then normalised with the maximum value of the respective reference case. The individual plots are placed in the order of increasing reduced frequency. At $k = 0.54$, the unsteady pressure decreases as the axial gap increases. This is consistent with a slightly increased reduced frequencies $k = 1.96$ and $k = 2.53$. However, the differences are significantly smaller here. Upon further increase in the reduced frequency to $k = 3.83$ and $k = 4.29$, the unsteady pressure suddenly increases with the gap. This trend changes back to the initial trend when the reduced frequency is further increased to $k > 5.55$. This low sensitivity of the pressure variation and the reversed response occur for $k \approx 2..4$, which corresponds to the area of low sensitivity of the aerodynamic work (Fig. 5).

The radial distributions of the aerodynamic work are shown in Fig. 7. This shows the low sensitivity of aerodynamic work across the span. As indicated by the arrows remarking the points of maximum deformation amplitude, the spanwise work distributions correspond to the respective leading-edge deformations (Fig. 2). Since the leading edges receive the highest unsteady pressure and the maximum deformation in the majority of cases, they contribute the most to the total aerodynamic work. In the case of predominantly bending modes, e.g., Mode 3 and Mode 6, an reversed trend of the vibrational response is likely because the stronger deformation at one point is cancelled by an opposite deformation at another point. The unsteady work may, therefore, behave differently from the unsteady pressure.

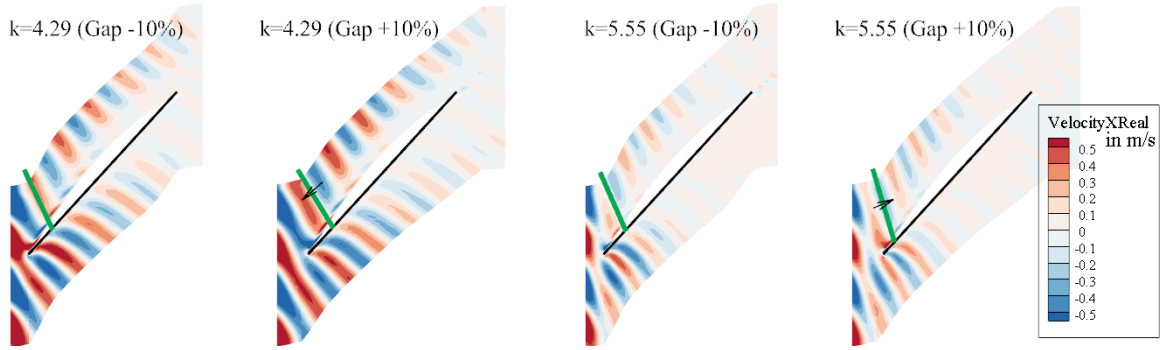

Figure 8 Real part of axial velocity at the midspan

Wake Propagation In Rotor Passages

As illustrated in Figure 6, the unsteady pressure increases with an increasing axial gap for $k = 4.29$, and decreases for $k = 5.55$. To explain why, the unsteady axial velocity distributions of these cases are shown in Figure 8. The contours are extracted at the midspan. Evidently, the wakes tilt as a result of this interaction with the potential field. As the axial gap increases, the angle between the wakes and the main flow increases as well, because the potential field of the rotor blade has more time to act upon the incoming wakes. The angle becomes perpendicular at $k = 4.29$ which results in the strongest propagation of the wakes through the rotor passage and an overall stronger unsteady pressure field. For the case of $k = 5.55$, this angle decreases when the wakes interact with the rotor potential field and cause a weaker propagation of the unsteady pressure field.

CONCLUSIONS

Numerous time-linearised forced-response simulations have been conducted to investigate the sensitivity of the forced response with respect to the operating point and mode shape. The main conclusions are as follows.

- The first harmonic of the inlet gust boundary condition exhibits by far the strongest sensitivity with respect to the axial-gap variations. This supports the validity of the linearisation approach chosen in this paper.
- The sensitivity of the unsteady aerodynamic work with respect to an axial-gap variation changes with the reduced frequency. Three distinct regimes were identified: moderate, low, and high sensitivity.
- The region of increasing sensitivity is caused by a steep increase in the sensitivity of the unsteady pressure with respect to an axial-gap variation.
- The identified regimes may prove to be important in the compressor-design stages in order to determine whether a certain compressor design is aeroelastically acceptable without performing 3D unsteady simulations. Further studies are, however, needed to generalise the numerical values determining these regimes.
- Predominantly bending modes are difficult to predict accurately from the mere unsteady-pressure field due to opposing contributions of different leading-edge deformations.
- Some reduced frequencies in the low-sensitivity regime exhibit a reversed sensitivity with respect to the axial gap. This effect can be explained by a change in the type of interaction between the incoming wakes and the rotor potential field: in any case, wakes propagate the strongest when their trajectories are perpendicular to the flow direction.
- The contribution of higher harmonics, as well as reflected and scattered waves, should be considered in future studies, e.g., by employing a harmonic-balance simulation approach.

NOMENCLATURE

c_x	rotor blade axial chord length
f	eigenfrequency
H	relative channel height
k	reduced eigenfrequency ($= fc_x/2V$)
s	blade surface
V	freestream axial velocity
w_F	aerodynamic work per area
W_F	aerodynamic work ($=\int w_F ds$)

ACKNOWLEDGEMENTS

We would like to acknowledge the funding by the Deutsche Forschungsgemeinschaft (DFG, German Research Foundation) under Germany´s Excellence Strategy EXC 2163/1 Sustainable and Energy Efficient Aviation Project ID 390881007. We would also like to acknowledge the contribution of the DLR Institute of Propulsion Technology and MTU Aero Engines AG for providing TRACE. We would like to acknowledge Mr. Torben Eggers and Professor Jens Friedrichs from Institute of Jet Propulsion and Turbomachinery, TU Braunschweig for providing the compressor configuration and steady-state solutions. We thank the Leibniz Universität Hannover IT Services (LUIS) for providing computational resources.

REFERENCES

Besem, F. M., Kielb, R. E., Galpin, P., Zori, L. and Key, N. L. (2016), 'Mistuned forced response predictions of an embedded rotor in a multistage compressor', *Journal of Turbomachinery* **138**(6).

Bittner, S. L., Keller, C., Meinzer, C. E. and Seume, J. R. (2018), Experimental validation of a forced response analysis using a time-linearized method, *in* '2018 AIAA/ASCE/AHS/ASC Structures, Structural Dynamics, and Materials Conference', American Institute of Aeronautics and Astronautics, Reston, Virginia.

Blocher, M. and Gómez Fernández, I. E. (2014), Time-linearized forced response analysis of a counter rotating fan: Part i — theoretical concept of a fully time-linear forced response analysis, *in* 'Volume 7B: Structures and Dynamics', American Society of Mechanical Engineers.

Chen, T., Rogerson, J. and Patel, K. (2013), Effects of both axial gap and blade count ratio on the forced response of a steam turbine stage, *in* 'Volume 5B: Oil and Gas Applications; Steam Turbines', American Society of Mechanical Engineers.

Eggers, T., Kim, H. R., Bittner, S., Friedrichs, J. and Seume, J. R. (2020), 'Aerodynamic and aeroelastic effects of design-based geometry variations on a low-pressure compressor', *International Journal of Turbomachinery, Propulsion and Power* **5**(4), 26.

Junge, L., Ashcroft, G., Jeschke, P. and Frey, C. (2015), On the application of frequency-domain methods to multistage turbomachinery, *in* 'Volume 2B: Turbomachinery', American Society of Mechanical Engineers.

Kersken, H.-P., Frey, C., Voigt, C. and Ashcroft, G. (2012), 'Time-linearized and time-accurate 3d rans methods for aeroelastic analysis in turbomachinery', *Journal of Turbomachinery* **134**(5).

Kielb, R. and Chiang, H.-W. (1992), Recent advancements in turbomachinery forced response analyses, *in* '30th Aerospace Sciences Meeting and Exhibit', American Institute of Aeronautics and Astronautics, Reston, Virigina.

Korakianitis, T. (1992*a*), 'On the prediction of unsteady forces on gas turbine blades: Part 1—description of the approach', *Journal of Turbomachinery* **114**(1), 114–122.

Korakianitis, T. (1992*b*), 'On the prediction of unsteady forces on gas turbine blades: Part 2—analysis of the results', *Journal of Turbomachinery* **114**(1), 123–131.

Manwaring, S. R. and Wisler, D. C. (1993), 'Unsteady aerodynamics and gust response in compressors and turbines', *Journal of Turbomachinery* **115**(4), 724–740.

Meinzer, C. E. and Seume, J. R. (2020), 'Experimental and numerical quantification of the aerodynamic damping of a turbine blisk', *Journal of Turbomachinery* **142**(12).

Schoenenborn, H. (2018), 'Analysis of the effect of multirow and multipassage aerodynamic interaction on the forced response variation in a compressor configuration—part i: Aerodynamic excitation', *Journal of Turbomachinery* **140**(5).